

Effect of pressure on the Raman modes of antimony

X. Wang,¹ K. Kunc,¹ I. Loa,¹ U. Schwarz,² and K. Syassen^{1, y}¹Max-Planck-Institut für Festkörperforschung, Heisenbergstrasse 1, D-70569 Stuttgart, Germany²Max-Planck-Institut für Chemische Physik fester Stoffe,

Notnitzer Strasse 40, D-01187 Dresden, Germany

(Dated: 28 August 2006)

The effect of pressure on the zone-center optical phonon modes of antimony in the A7 structure has been investigated by Raman spectroscopy. The A_g and E_g frequencies exhibit a pronounced softening with increasing pressure, the effect being related to a gradual suppression of the Peierls-like distortion of the A7 phase relative to a cubic primitive lattice. Also, both Raman modes broaden significantly under pressure. Spectra taken at low temperature indicate that the broadening is at least partly caused by phonon-phonon interactions. We also report results of ab initio frozen-phonon calculations of the A_g and E_g mode frequencies. Presence of strong anharmonicity is clearly apparent in calculated total energy versus atom displacement relations. Pronounced nonlinearities in the force versus displacement relations are observed. Structural instabilities of the Sb-A7 phase are briefly addressed in the Appendix.

PACS numbers: PACS: 78.30.-j, 63.20.-e, 71.15.Nc, 62.50.+p

I. INTRODUCTION

Like other semimetals of the group V-A, antimony crystallizes at ambient conditions in the trigonal A7 structure (space group $R\bar{3}m$, No. 166).¹ Antimony is known to transform at 8.5 GPa to a high-pressure phase² that is referred to as Sb-II in the recent literature. At 28 GPa Sb converts to the body-centered cubic modification Sb-III.^{3,4} Diffraction studies^{5,6} show Sb-II to adopt a tetragonal self-hosting structure with an incommensurate guest-host arrangement. In addition, incommensurate modulations occur in Sb-II.⁶ The structural sequence for Sb under pressure is further complicated by the observation of another incommensurate phase, called Sb-IV, in a narrow pressure range from 8 to 9 GPa (up-stroke), i.e. intermediate between Sb-I and Sb-II.^{7,8}

Here we are interested mainly in the effect of pressure on optical phonon modes of the A7 phase of Sb. The A7 structure (Fig. 1) is a rhombohedrally distorted variant of a cubic primitive structure. The formation of paired layers results in a doubling of the number of atoms in the primitive rhombohedral cell. In this context, the term Peierls distortion is appropriate because the pairing is driven by a gain in electronic energy (formation of a pseudo-gap in the electronic density of states at the Fermi level E_F) which outweighs the cost in Ewald energy.⁹ In the following we will mostly refer to the hexagonal description of the structure. The non-primitive hexagonal unit cell contains six atoms. For conversion relations between rhombohedral and hexagonal cells we may refer to Ref. 10 or 11.

Group theory for the A7 structure predicts three zone-center optical modes, i.e. a singly degenerate A_{1g} mode (totally symmetric) and a doubly degenerate E_g mode. The atoms are displaced along the C_3 axis in the A_{1g} mode and perpendicular to that axis in the E_g mode. The A_{1g} mode is the 'Peierls distortion mode'. In the unfolded Brillouin zone of the cubic primitive structure, the

A_{1g} mode corresponds to a longitudinal acoustic mode at the R-point, whereas the E_g mode corresponds to a transverse acoustic mode at R.

Previous Raman studies of antimony at ambient pressure have addressed the resonance effects,¹² the second-order scattering by optical modes,¹³ the effect of temperature on the first-order modes,¹⁴ and the coupling of the first-order Raman modes to electronic excitations.¹⁵ The coherent A_{1g} phonon generation in Sb by short laser pulses is the subject of several more recent reports.¹⁶ Raman experiments on Sb under pressure were performed

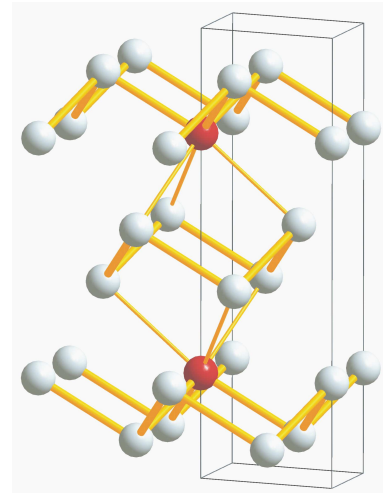


FIG. 1: (Color online) The A7 structure of Sb. Two distortion modes lead from the parent cubic-primitive (cP1) to the A7 (hR2) structure: a rhombohedral elongation along a cubic [111] direction and a pairing of the original cubic (111) lattice planes. Atoms in red mark opposite corners of the distorted cube. The resulting layered structure has a 3+3 atomic coordination. The non-primitive hexagonal unit cell is indicated in the figure.

by Richter et al.¹⁷ who measured frequency shifts up to 0.6 GPa and observed a softening of the zone-center optical modes, not only for Sb, but also the A7 phases of As and Bi. Optical phonons in As were studied up to 30 GPa using Raman spectroscopy¹⁸ whereas in the case of Bi femtosecond pump and probe techniques were applied to explore the effect of pressure up to 3 GPa on the modulation of the optical response by coherent A_{1g} phonons.^{19,20}

In this work, we have investigated the full stability range of the A7 phase of Sb using Raman spectroscopy. We also report Raman spectra of Sb-II measured up to 16 GPa. Our discussion focuses on results for the A7 phase, specially the pressure-induced softening of mode frequencies up to the first phase transition and the observed strong pressure dependence of the Raman line widths. Experimental results for phonon frequencies of the A7 phase are compared to frozen-phonon calculations performed within the density functional framework using optimized structural parameters. A side aspect of our calculations concerning structural instabilities of the A7 phase in the vicinity of the Sb-I to Sb-II transition is presented in the Appendix.

II. RAMAN SPECTROSCOPY

The Raman scattering measurements were performed on crystalline antimony of 99.999% purity. A diamond anvil cell (DAC) was used for pressure generation. Experiments were initially performed with nitrogen as a pressure medium and then, in order to avoid the Raman scattering of solid nitrogen,²¹ continued with the standard 4:1 m ethanol-ethanol mixture (M/E) as well as with helium; the latter ensures the best hydrostatic conditions in combination with low background. In all experiments, pressures were measured by the ruby luminescence method.^{22,23} Raman spectra as a function of pressure were recorded in backscattering geometry (normal of the sample surface parallel to the C₃ axis) using a triple-grating spectrometer (Jobin-Yvon T64000) in combination with a liquid-nitrogen-cooled charge-coupled device (CCD) detector. The resolution was set to $< 2 \text{ cm}^{-1}$. An argon ion laser was used for excitation at a wavelength of 514.5 nm. The laser was focused to a spot of 50 μm in diameter. The power incident at the sample surface was 15–20 mW. At that power level we did not notice any indication for laser-induced heating of the sample when mounted inside the DAC.

Figure 2 shows a subset of Raman spectra of antimony measured at room temperature and at different pressures up to 16.5 GPa. Spectra at 0, 2, and 5.6 GPa are for the A7 phase, those at 8.3 and 9.1 GPa are for phase mixtures, and those above 10 GPa are for Sb-II. The frequencies of the two observed Raman modes of the A7 phase decrease with increasing pressure. The A_{1g} feature is slightly asymmetric at low pressure, and with increasing pressure a shoulder develops at its high energy side.

A broad feature between 235 and 320 cm^{-1} seen at ambient pressure can be attributed to second-order scattering by optical phonon modes.¹³ Under applied pressure, that feature could not be separated well enough from the background scattering to allow for useful information to be obtained.

Schwarz et al.⁶ pointed out that the transition to Sb-II is sluggish and that a pure phase Sb-II can be obtained only above 13(1) GPa. On the other hand, Degtyareva et al. obtained a pure phase Sb-II at 9.1(1) GPa (upstroke). Our Raman spectra from different runs indicate a transition regime extending from about 8 to 10 GPa.

After passing the transition regime, the Raman spectra look quite different from those of the A7 phase. At least three new Raman features appear as indicated by the arrows in Fig. 2. All of them shift to higher frequency with increasing pressure. We could not reproducibly identify other distinct Raman features of Sb-II, except for a broad shoulder on the high energy side of the most intense Raman peak.

It has been reported that, at ambient pressure, the E_g and A_{1g} Raman features exhibits a Fano-like line

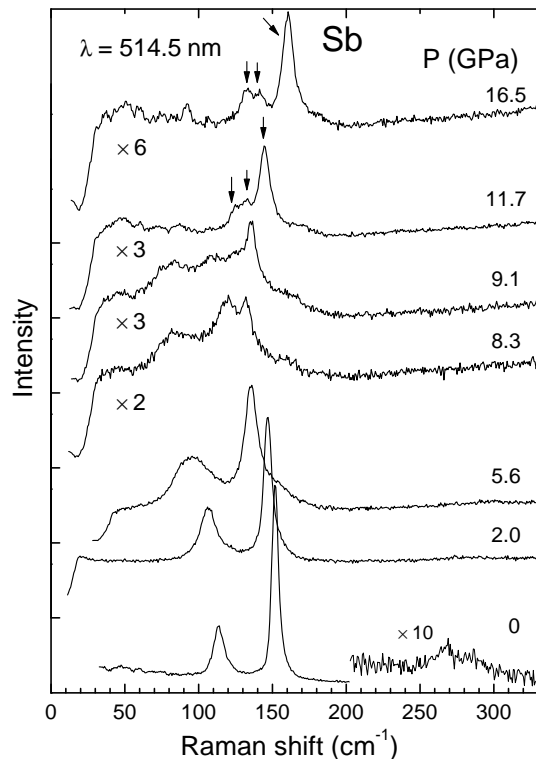


FIG. 2: Raman spectra of antimony at different pressures ($T = 300 \text{ K}$). Spectra are scaled to about the same maximum intensity; the scaling factors are given in the figure. The broad feature seen at about 270 cm^{-1} (see blown-up section of the bottom spectrum) is attributed to second-order Raman scattering of the A7 phase. The spectra at 8.3 GPa and 9.1 GPa correspond to a phase mixture of A7 and high pressure phase(s), those at 11.7 and 16.5 GPa to Sb-II. A weak Raman feature characteristic of Sb-II.

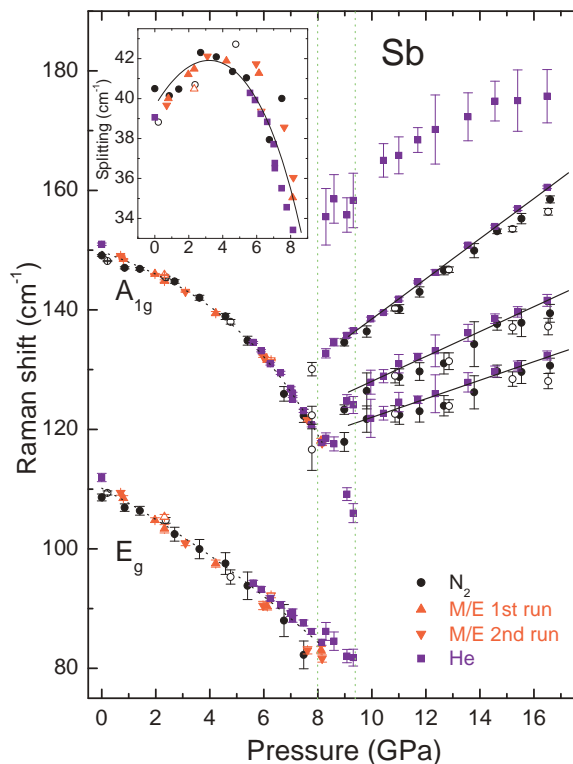


FIG. 3: (Color online) Raman peak frequencies of Sb as a function of pressure at room temperature. Closed symbols are for increasing pressure, open symbols for decreasing pressure. Data were collected in runs using different pressure media. The transition regime between the A7 phase and phase II is indicated by vertical dashed lines. Lines passing through the data points represent results of least squares fits (for parameters see Table I). The inset shows the splitting of the optical mode frequencies of the A7 phase as a function of pressure. There, the line is a guide to the eye.

shape which is believed to arise from the interaction between electronic intraband scattering and one-phonon scattering.¹⁵ These asymmetries are weak, however. So, for the purpose of extracting peak positions and approximate line width parameters from the Raman data for the A7 phase, a fitting by symmetric pseudo-Voigt line shapes was found to be adequate. For Sb-II, peak frequencies were determined by simply locating intensity maxima. The obtained frequencies of Raman features of Sb for pressures up to 16 GPa are shown in Fig. 3. Within the scatter of the frequency data, the pressure effects are fully reversible.

The observed ambient-pressure A_{1g} and E_g mode frequencies are 149.8 cm^{-1} and 110 cm^{-1} at room temperature [values measured for one of the samples at 2 K are $155.7(7)$ and $117.0(3) \text{ cm}^{-1}$]. For a pressure of 7.5 GPa, the total relative shift is -18% and -24% for the A_{1g} and E_g modes. The magnitude of these shifts is similar to what has been found for the optical modes of arsenic in the more extended stability range ($0 \leq P < 25 \text{ GPa}$) of its A7 phase.¹⁸ The nonlinear $\omega(P)$ behavior of the E_g mode of

TABLE I: Frequencies of the Raman features of the Sb-A7 and Sb-II phases. The pressure dependence is described by $\omega(P) = \omega_0 + aP + bP^2 + cP^3$ where frequency ω is in cm^{-1} and pressure P in GPa. For the Sb-I phase, the zero-pressure frequencies ω_0 , the linear pressure coefficients A , the quadratic one (B) for the E_g mode, and the cubic coefficient C for the A_{1g} mode are given. The zero-pressure mode Grüneisen parameters γ_0 are determined from the linear coefficients a and the reported bulk modulus $B_0 = 39.7 \text{ GPa}$.⁸ For the Sb-II phase, we list Raman peak frequencies ω at 9.1 GPa and the average linear coefficients \bar{a} for the pressure range from 9 to 16 GPa. The average values $\bar{\gamma}$ of the mode Grüneisen parameter given for that range are estimated assuming a bulk modulus value of 100 GPa.

A7	Mode	ω_0	a	b	c	γ_0
	E_g	110(1)	-2.4(6)	-0.10(7)	0	-0.58
	A_{1g}	149.8(10)	-1.8(3)	0	-0.032(3)	-0.48
Sb-II		Mode ω (9.1 GPa)	\bar{a}			
	1	121(2)	1.6(1)	1.3		
	2	126(2)	2.1(1)	1.65		
	3	135.6(5)	3.36(4)	2.45		

Sb can be described by the usual combination of a linear and quadratic pressure coefficient, that of the A_{1g} mode is approximated well by a combination of a linear and a cubic term in pressure. Sets of polynomial parameters characterizing the pressure dependence of mode frequencies and mode Grüneisen parameters are given in Table I.

The frequencies of the Raman bands attributed to the phase Sb-II are 121, 126, and 135.6 cm^{-1} at 9.1 GPa. The frequencies of all three features exhibit an essentially linear pressure dependence up to 16 GPa. The corresponding mode Grüneisen parameters $\bar{\gamma}$ given in Table I were estimated using a bulk modulus value of $B_0 = 100 \text{ GPa}$ as extracted from pressure-volume data given in Ref. 7.

The structure of Sb-II consists of an incommensurate guest-host arrangement. For the host structure with tetragonal symmetry and space group $I4mm$, a group theory analysis gives five zone-center Raman-active modes of symmetry A_{1g} , B_{1g} , B_{2g} , $E_g(1)$, and $E_g(2)$. The corresponding displacement patterns are those of the aluminum sublattice in CuAl_2 .²⁴ Only three Raman features could be clearly identified in our spectra for Sb-II. Not having investigated polarization effects, we do not propose an assignment at this point. So, concerning Sb-II, the main result of the present study is that the frequencies of Raman peaks presumably due to optical phonons are similar to that of the A_{1g} mode of Sb-I and, different from Sb-I, the optical phonons of Sb-II harden with increasing pressure and the values of the mode Grüneisen parameters are larger than one.

In view of the observed changes in the phonon frequencies under pressure, we briefly mention two related properties of Sb. First, there is the negative slope of the melting line of Sb-I. The melting temperature drops from 904 K at ambient to about 830 K at 5 to 5.7 GPa (the triple

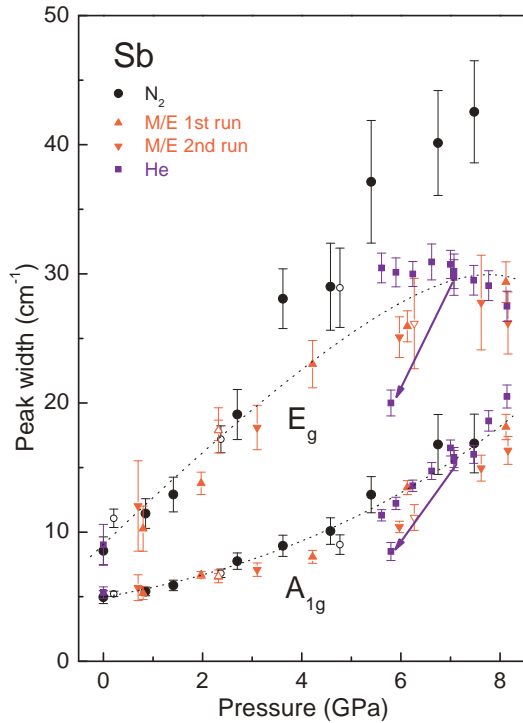


FIG. 4: (Color online) Raman line widths (FWHM) of A7 antimony as a function of pressure at room temperature. Different shapes of symbols are used for different pressure media. Closed symbols are for increasing pressure, open symbols for decreasing pressure. Dashed lines are guides to the eye. Note that the pressure-induced broadening is fully reversible. Arrows indicate the change in width upon cooling to 5 K (cf. spectra shown in Fig. 5).

point between liquid, Sb-I and high pressure phase).^{25,26} Within a 'single-phase' approach to melting and in the spirit of the Lindemann melting criterion, a microscopic explanation of the negative melting slope would have to take into account that at least part of the phonon spectrum softens considerably with increasing pressure. The second remark concerns the pressure-induced superconductivity of antimony. The superconducting transition temperature T_c of Sb-I increases with increasing pressure, reaching 0.7 K at 8.5 GPa.²⁷ At the phase transition to Sb-II, T_c jumps to 3.7 K and then it drops continuously to 2 K at 25 GPa.²⁷ Qualitatively, the increase of T_c in the A7 phase can be understood to arise from an increase of the density of states $N(E_F)$ (i.e. the filling of the pseudogap, cf. Refs. 28 and 29) and, in view of the strong phonon softening, an enhanced electron-phonon coupling.⁹ In the phase Sb-II, $N(E_F)$ is much larger compared to that of Sb-I at ambient pressure.^{28,29} The effect of pressure on $N(E_F)$ of Sb-II appears to be not very pronounced.²⁹ So, one can speculate that a hardening of relevant phonon modes, as indicated by our Raman data for optical modes, accounts for the decrease of T_c with increasing pressure in Sb-II.

Besides a large phonon softening in Sb-I, the second

very pronounced effect of pressure is the change in line widths of the A_{1g} and E_g Raman peaks. The pressure dependence of the peak widths (FWHM) is shown in Fig. 4. Error bars take into account some ambiguity in separating a peak from the background and/or shoulders. Between ambient pressure and 8 GPa, the width of the A_{1g} feature increases by about a factor of three, from 6 cm^{-1} to 17 cm^{-1} . The E_g -related peak starts with a width of 9 cm^{-1} at ambient and the width increases substantially to 30 cm^{-1} at 8 GPa. For the N_2 medium (solid at 2.5 GPa and changing phase at 6 GPa), the width becomes even larger under pressure; so, the observed line width of the E_g feature seems to depend sensitively on non-hydrostaticity or shear strength of the pressure medium. The data obtained with alcohol and helium medium are considered to reflect the effect of truly hydrostatic stress on the Raman line widths. It is important to note that the pressure-induced broadenings were found to be fully reversible within experimental scatter. This also applies to runs which, during upstroke, passed into the Sb-II phase regime.

We have performed one high-pressure experiment at low temperature. The sample was loaded in He medium, taken to 7.1 GPa at 300 K, and then cooled to 5 K. During cooling the pressure dropped somewhat to 5.8 GPa due to experimental factors. The high-pressure spectra at 300 K and 5 K are shown in Fig. 5, together with room- and low-temperature spectra measured at ambient pres-

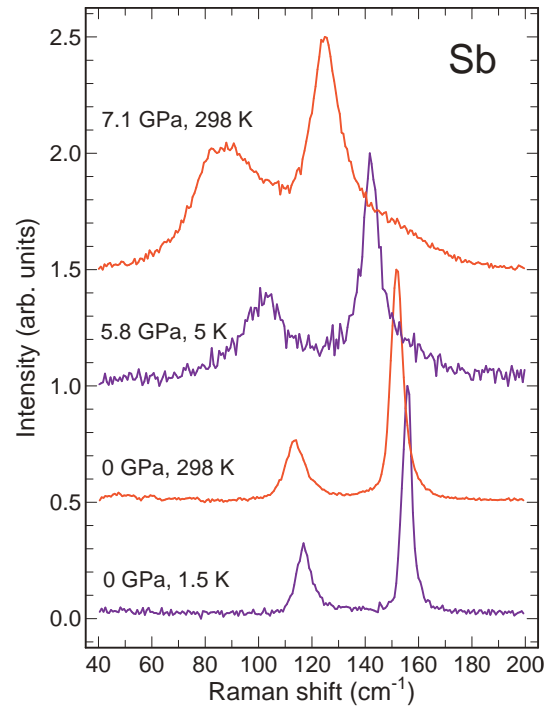


FIG. 5: (Color online) A room-temperature Raman spectrum of Sb at 7.1 GPa compared to the spectrum measured after cooling to 5 K. Upon cooling, the pressure dropped to 5.8 GPa. Spectra were measured for a helium pressure medium.

sure. At zero pressure and when cooling, the width of the A_{1g} drops from 5.4 to 4.1 cm^{-1} , that of the E_g mode from 8.9 to 6.6 cm^{-1} . The low-temperature widths are larger compared to those reported in Ref.,¹⁴ presumably due to crystal imperfections induced by the sample preparation procedures. At high pressure the change in width is 14 ± 8.5 cm^{-1} for A_{1g} and 28 ± 20 cm^{-1} for E_g . The latter changes are indicated by arrows in Fig. 4. These changes in peak widths demonstrate that about half of the phonon decay rate at room temperature is thermally activated. Spectral weight components like the shoulder on the high-frequency side of A_{1g} also depend on temperature.

A possible explanation of the line widths changes under pressure would be the coupling to acoustic phonons via cubic anharmonicity.^{14,30} At ambient pressure, the E_g mode frequency represents the lower frequency limit of the optical phonon branches, separated by about 10 cm^{-1} from the acoustic mode regime.¹⁰ Based on the experimental phonon dispersion relations,¹⁰ one can expect a large two-phonon density of states (DOS) for acoustic modes spanning the range from about 80 to 160 cm^{-1} . So, decay of the zone-center optical phonons into two acoustic modes should be energetically possible. In view of the optical phonon softening and related strong anharmonicity (see also discussion below), an increase of the third-order coupling strength under pressure may be the dominant effect causing the line broadening. At this point we hesitate to elaborate further on this scenario, because we don't know the effect of pressure on the two-phonon DOS and, furthermore, pressure-induced changes in electronic structure should be considered as well.

At ambient pressure, antimony is a semimetal with a negative indirect gap of 0.1 eV. The free carriers (density $10^{20}/\text{cm}^3$) occupy states at Brillouin zone edges, forming pockets with small effective masses.^{31,32,33} A coupling between the optical phonon modes and low-energy electronic excitations appears to be supported by a Raman study.¹⁵ Now, the pseudogap of Sb is expected to change significantly (towards closing up) under pressure, leading to a major change in the coupling of phonons to electronic states near the Fermi level.⁹ Furthermore, the response in the visible spectral range may be affected also, in particular the so-called E_2 transition near 2.5 eV³⁴ which at ambient pressure is in resonance with the exciting laser energy used in this study. So, we cannot neglect effects related to the penetration depth of the laser light.³⁵ Furthermore, resonance conditions for Raman scattering may also change.

III. PHONON FREQUENCY CALCULATIONS

The phonon frequency calculations presented here are based on an evaluation of the total energy within the Density Functional Theory (DFT).^{39,40} We work in a plane-wave basis and use the Projector Augmented Waves (PAW) method^{41,42} as implemented in the VASP

TABLE II: Structural parameters of Sb-I obtained from DFT calculations using the LDA and GGA schemes. The values refer to the respective calculated zero-pressure volumes. The lattice parameters are for the non-primitive hexagonal cell, the volumes are for the primitive unit cell (2 atoms). The calculated values of bulk modulus B_0 and its pressure derivative B_0' were obtained by fitting a third-order Birch equation of state to the calculated pressure-volume data (the attached errors reflect parameter correlations). Related experimental results are listed in the lower part of the table.

	a (Å)	c=a	u	V_0 (Å ³)	B_0 (GPa)	B_0'
LDA	4.3003	2.5406	0.2368	58.32 (1)	46.7 (6)	4.9 (3)
GGA	4.3779	2.6209	0.2334	63.48 (3)	34.4 (6)	5.4 (2)
4 K	4.3007 ^a	2.6093 ^a	0.23362 ^a	59.918		
298 K	4.3084 ^a	2.6167 ^a	0.23349 ^a	60.41	39.7 ^b	4 ^b
298 K					45.6 ^c	
298 K					40.2 ^d	

^a X-ray diffraction, Ref. 36

^b X-ray diffraction, B_0' fixed, Ref. 8

^c Ultrasonic wave velocities, Ref. 37, adiabatic value

^d Ultrasonic wave velocities, Ref. 38, adiabatic value

codes.⁴³ The (pseudo-) potential^{41,42} of Sb was available from G. Kresse and J. Joubert.⁴² Scalar relativistic corrections are taken into account indirectly, through the construction of the (pseudo-)potential. The expansion of wave-functions includes plane-waves with kinetic energies up to the cutoff energy of $E^{PW} = 215$ eV. As antimony is metallic, we used for the Brillouin zone sampling a relatively dense uniform $14 \times 14 \times 14$ mesh which corresponds to 280 k-points in the irreducible wedge.⁴⁴ In order to deal with the partially occupied orbitals we employed the method of Methfessel and Paxton⁴⁵ (to the first order) with a smearing parameter $\sigma = 0.1$ eV. Whenever pressures are quoted in the context of calculations, they were obtained from the DFT directly using the stress theorem.⁴⁶ We have tested the LDA and GGA versions⁴⁷ of the (pseudo-)potential (essentially we repeated all structural calculations (such as the $E(V)$ and $P(V)$ equations of state) in both LDA and GGA. Neither of the two approximations turned out to be convincingly superior to the other and most of the phonon calculations reported below relate to LDA unless stated otherwise.

The phonon frequencies were calculated in the frozen phonon approach starting from optimized structural parameters. Our optimized structural parameters at zero pressure (calculated) are given in Table II. Results of structure optimizations at different volumes are discussed in the Appendix.

The frozen-phonon approach consists in the evaluation of the total energy E^{tot} of the crystal with frozen-in atomic displacements. Small displacements $v(1) = (0;0;v)$ and $v(2) = (0;0;v)$ in the A_{1g} mode and $v(1) = (v;0;0)$ and $v(2) = (v;0;0)$ in the E_g mode were applied to the two atoms of the basis, and the two

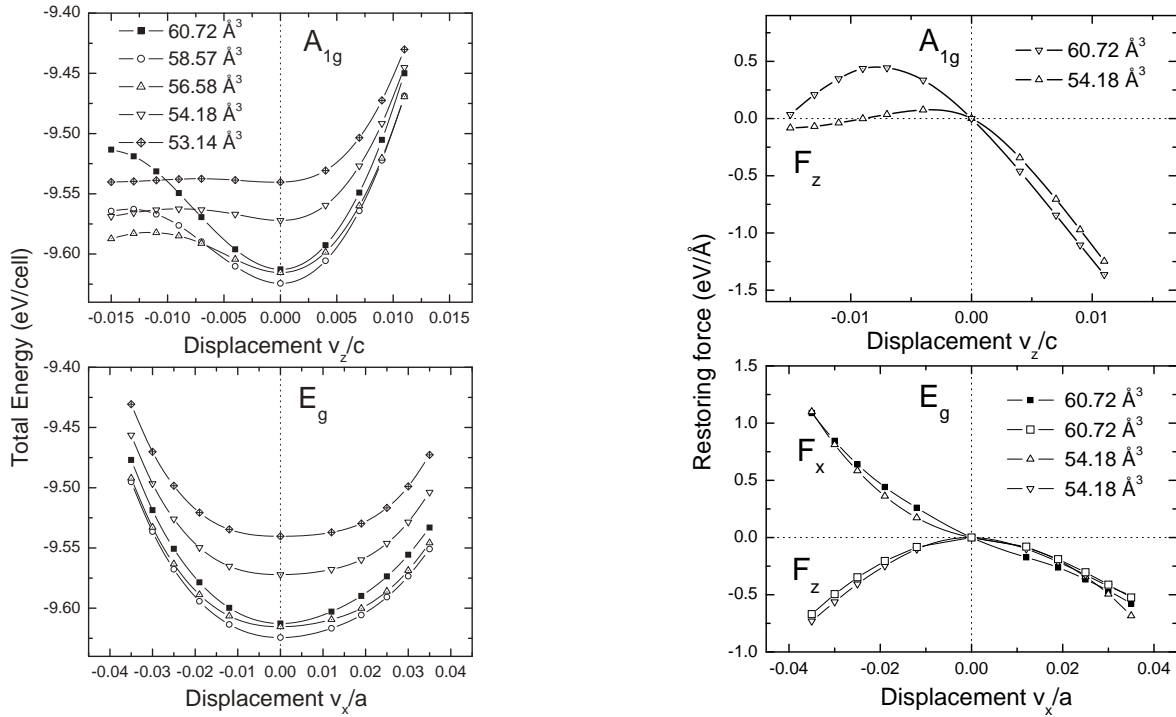


FIG. 6: Results of total energy calculations (LDA) for Sb in the A7 structure. Left: Energy at different volumes as a function of phonon displacement for the A_{1g} and E_g modes. In the order of decreasing volume, the calculated pressures are 1.68, 1.52, 1.52, 4.14, and 5.46 GPa. In the A_{1g} mode, the positive displacement corresponds to the shortening of the covalent Sb(Sb) bond. Left: Restoring forces as a function of displacement for the A_{1g} and E_g modes at two different volumes. In the case of the E_g mode, both the forces in x and z direction are given ($F_y = 0$ at all volumes). For the A_{1g} mode, there is no non-parallel force component.

values obtained for E^{tot} [viz. the E^{tot} (outward) and E^{tot} (inward)] were averaged. The eigenfrequency is then obtained from the expression for the energy of a harmonic oscillator

$$E^{\text{tot}} = \frac{1}{2} M \dot{y}^2 - \frac{1}{2} k y^2 + \frac{1}{4} \alpha y^4; \quad (1)$$

where M is the atomic mass of Sb. As all the $E^{\text{tot}}(v)$ variations suggested presence of anharmonic terms we chose the values of $v_z/c = 0.004$ (for A_{1g}) and $v_x/a = 0.012$ (for E_g) at which the eventual quartic terms are negligible. The main anharmonic terms to take care of are the cubic ones, and they are eliminated by averaging the E^{tot} (outward) and E^{tot} (inward).

Presence of the anharmonicity in the $E(v)$ potential is clearly visible in Fig. 6. The scales of v are about the same for the A_{1g} and E_g mode when measured in absolute displacements (0.1 Å corresponds, at ambient pressure, to $v_z/c = 0.0089$ or $v_x/a = 0.023$). We can see that, at low pressures, the energy variation in the E_g mode does not differ much from a parabolic shape: the main deviation shows as the slight asymmetry for positive and negative v . The degree of asymmetry remains about the same when pressure is increased. This behavior is in stark contrast with the one seen in the A_{1g} mode where, at $P = 0$, the $E(v)$ is essentially symmetric at small displacements ($v/c \approx 0.005$) but its asymmetry rapidly

increases under compression, to reach at $V = 53.14 \text{ \AA}^3$ ($P = 5.5 \text{ GPa}$) an almost flat shape in one of the displacement directions.

A closer inspection of the A_{1g} potential energy curves reveals, at low pressures ($P = 1.58 \text{ GPa}$), a small energy barrier around $v_z/c \approx 0.01$; when pressure increases the barrier shifts to smaller values of v_z/c and becomes lower. An expansion of the unit cell, on the contrary, makes the barrier higher and shifts its position to larger values of the displacement (e.g. $v_z = 0.015c = 0.17 \text{ \AA}$ at $P = 1.68 \text{ GPa}$), where it is beyond the reach of the mean-square displacement at room temperature ($v_z \approx 0.09 \text{ \AA}$). It should be noted that the maximum of the barrier corresponds to the structural parameter $u = 0.25$. If we had plotted the results by measuring the displacement v_z relative to $u = 0.25$, we would have obtained symmetric potential energy curves similar to those shown in Refs. 9 (Sb) and 48 (Bi).

More comprehensive information about the anharmonicity is provided by the variation of forces with displacements, which is also plotted in Fig. 6. Now the anharmonic regime is easily recognized by the linear variation of the restoring force F against v . At all volumes close to ambient pressure the A_{1g} mode is harmonic, until approximately the displacements of $v_z/c = 0.004$, which is the value we chose for the frozen phonon calculations,

to become conspicuously anharmonic at $V = 54.18 \text{ \AA}^3$ ($P = 4.1 \text{ GPa}$). For the E_g mode, on the other hand, the F_x seems to deviate little from the linear (i.e. harmonic) behavior for $v_x = a \approx 0.02$, even when pressure is increased. However, and perhaps to some surprise at the first sight, a component of force $F_z \neq 0$ appears in this mode.

This somewhat unexpected emergence of the non-parallel component F_z reminds us that a multitude of different anharmonic terms can appear in the expansion of $E(v)$, and the presence of anharmonicity then can show up in two ways: (1) forces are not linear in v and (2) forces are not necessarily parallel to the displacement (see Ref. 49, Sect. III). It is the "mixed" $v_x v_z$ terms in

$$\begin{aligned} E^{A_{1g}}(v_z) &= A v_z^2 + B v_z^3 + C v_z^2 v_x + D v_z v_x^2 + \dots \\ \text{or} & \\ E^{E_g}(v_x) &= A v_x^2 + B v_x^3 + C v_x^2 v_z + D v_x v_z^2 + \dots \end{aligned} \quad (2)$$

that are responsible for the "non-parallelism" of F and v . Figure 6 shows that, while the "parallel" term B seems to be significant in A_{1g} , it is the large C which gives rise to the non-zero component F_z in E_g . Dealing only with the $E(v)$ variations (Fig. 6) would, obviously, make us miss any mixed term in Eqs. (2).

In the harmonic regime, using the Hellmann-Feynman forces merely offers a convenient, alternative way to ex-

plore the calculated $E(v)$ data. However, in an anharmonic oscillator the knowledge of the variation $F(v)$ provides us with additional information on the mixed terms in Eqs. (2).

In the light of the above discussion, it does not come as a surprise finding out that the harmonic frequencies calculated from Eq. (1) agree rather in perfectly with the measured data shown in Fig. 7. However, the overall trend of the variation is correctly reproduced. In particular, the initial rate of the variation with volume is not far from the observed values and the larger nonlinearity in the softening of A_{1g} mode is reproduced also. The discrepancies remind us that the (calculated) harmonic frequencies are not the quantity that is measured in the spectrum of an anharmonic oscillator. Another contribution to the discrepancy is caused by a deviation of the optimized c/a ratios from experimental values (see Appendix).

An attempt to evaluate the frequency shifts or the line-broadenings in terms of some of the theories proposed in the past⁵⁰ would lead us beyond the scope of this paper. In particular, one would have to assume that anharmonicity is the only mechanism responsible for the 20 cm^{-1} shifts appearing in Fig. 7, which is by no means certain.³⁵

IV. CONCLUSIONS

We have performed a high pressure Raman scattering study of Sb up to 16.6 GPa at room temperature. On the approach to the Sb-I to Sb-II phase transition near 8 GPa, both the A_{1g} and E_g zone-center phonon modes of the A7 phase exhibit a pronounced softening, of the order $\sim 20\%$. Frozen-phonon calculations yield harmonic phonon frequencies in reasonable agreement with the observed mode softening. The two Raman lines of the A7 phase show an unusually large broadening under pressure. The fact that the lifetime of phonons decreases with increasing pressure could become important if, similar to Bi,^{19,20} the effect of pressure on coherent phonon generation in Sb were to become of interest. We report Raman-active modes of the phase Sb-II which has a complex guest-host structure. For the Sb-II phase, all the observed phonon features exhibit a hardening with increasing pressure, at least up to 16 GPa; a correlation with the negative pressure coefficient of the superconducting transition temperature of Sb-II²⁷ is apparent.

Perhaps the most interesting question raised by the present study concerns the coupling of the zone-center optical phonons of the A7 phase of Sb to other phonons (e.g. anharmonic decay) and possibly electronic processes (electron-phonon coupling). It is the interplay between mode softening, electronic structure changes at the Fermi level, and shifts of optical interband transitions (i.e. resonances and penetration depth) which leads to a more complex scenario of phonon decay processes compared to semiconducting materials. Our low-

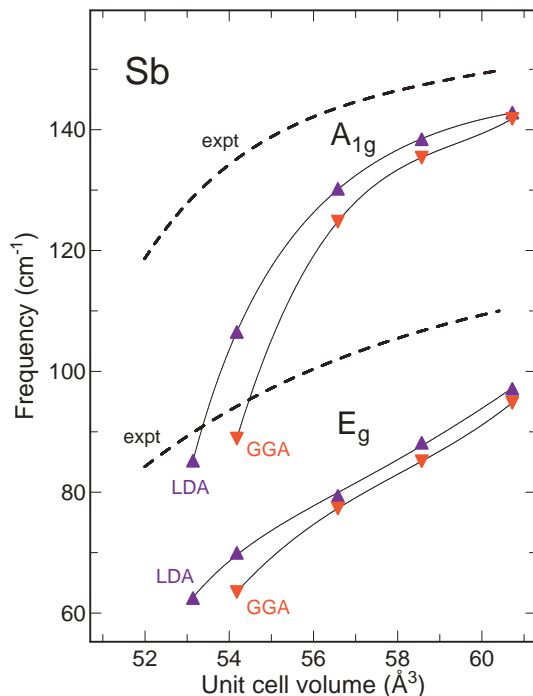


FIG. 7: (Color online) Results of frozen-phonon calculations (LDA and GGA) for Sb in the A7 structure: harmonic phonon frequencies at different unit cell volumes. The experimental data (dashed lines) are indicated for comparison. Experimental pressure is converted to volume using a Birch equation of state with experimental parameters given in Table II.

temperature measurements of the Raman line widths indicate that phonon-related processes are a major cause of the pressure-induced broadening. So, a first step towards gaining more insight would be to study the effect of pressure on the phonon dispersion relations, especially the acoustic branches.

APPENDIX A: A7 STRUCTURE OPTIMIZATION

The literature about different phases of antimony includes several studies based on first-principles calculations.^{6,9,28,51} An interesting problem had been the question of the existence of a cubic primitive (cP1) structure of Sb at pressures between 6 and 9 GPa. The cP1 structure can be viewed as a special case of A7 with $u = 0.25$ and $c/a = \sqrt{6}$. First suggested experimentally in Ref. 52, the reality of the cP1 phase was not confirmed in later diffraction studies of Sb, e.g. Refs. 2,6,8. Since then the A7 \rightarrow Sb II/IV transition is believed to be the first in the sequence of pressure-induced transitions of Sb, and the 'cubic-primitive' subject has occasionally appeared only in theoretical studies which slowly "converged" to elimination, on energetic grounds, of the cP1 phase from the list of stable phases of antimony.

Our calculated results for the optimized structural properties of Sb-A7 as a function of unit cell volume, in part sampled at very small volume intervals of 0.1 \AA^3 , are summarized in Fig. 8. Let's first consider the LDA results. Starting from large volume, the calculated variation $P(V)$ [Fig. 8(a)] is smooth first. When passing $V = 52.9 \text{ \AA}^3$ a kink appears in $P(V)$, followed by narrow interval of smooth variation, until $V = 52.1 \text{ \AA}^3$. The kink in $P(V)$ relates to the evolution of the structural parameters c/a and u [Figs. 8(b,c)]. At the approach to $V = 52.9 \text{ \AA}^3$ the smooth decrease of c/a changes slope and c/a takes, practically discontinuously, values situated close to the cubic value $c/a = \sqrt{6}$. At the same volume, a nearly abrupt variation towards the cubic limit $u = 0.25$ is also observed in the behavior of u . However, the cubic limit of u is only reached by a second 'jump' near $V = 52.1 \text{ \AA}^3$. At all volumes $V > 52.1 \text{ \AA}^3$, the energy-minimization algorithms, set to conserve the $R\bar{3}m$ symmetry, steer the iteration obstinately towards exactly $u = 0.25$, but with c/a significantly larger again than the cubic value $c/a = \sqrt{6}$. When increasing the volume from below to above $V = 52.1 \text{ \AA}^3$, the optimization procedure tends to stay trapped at $u = 0.25$ until at about $V = 54 \text{ \AA}^3$ it falls back to the curve obtained for decreasing volume.

The corresponding $E(V)$ calculations (not shown here) tell us that the range $V \in (52.1; 52.9) \text{ \AA}^3$ (P^{LDA} between 5.7 and 6.6 GPa) should be considered as the region of co-existence of two A7 variants, because the total energy differences are smaller than 2 meV/cell and the specific volumes are almost identical. The third A7 variant is energetically favored for $V < 52.1 \text{ \AA}^3$ ($P^{\text{LDA}} < 6.6 \text{ GPa}$). However, at these volumes the A7 \rightarrow Sb-II transition (not

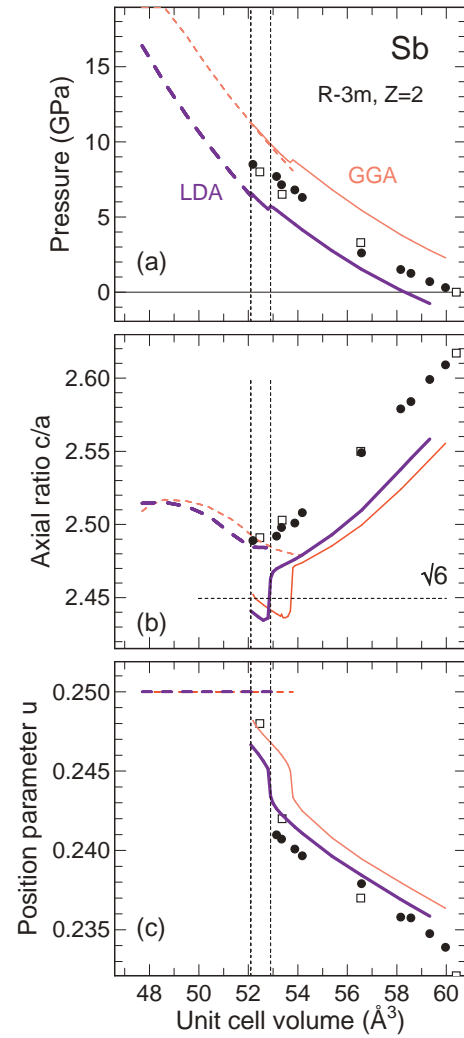


FIG. 8: (Color online) Calculated structural properties of Sb in the A7 structure as a function of rhombohedral unit cell volume (2 atoms per cell): (a) equation of state $P(V)$; (b) axial ratio c/a ; (c) positional parameter u . In the LDA approximation, a sequence of two structural transitions to variants of the A7 structure (see text) is predicted between $V = 52.9$ and 52.1 \AA^3 (marked by dashed vertical line). In GGA, the corresponding volume range is larger. Closed circles and open squares represent the tabulated experimental results.^{2,7} The dashed vertical line at 52.1 \AA^3 coincides with the smallest volume for which the pure A7 phase has been observed experimentally at 300 K .²

investigated here) is even more favored; the experiments² situate the appearance of the latter phase at $V = 52.2 \pm 0.02 \text{ \AA}^3$. Hence, the possibility of observing that third A7 variant can be ruled out.

The peculiar variations of c/a and u at $V = 52.9 \text{ \AA}^3$ indicate a transition to a pseudo-cubic A7 variant where only the metric approaches the cubic value ($c/a = \sqrt{6}$). The symmetry of the structure remains $R\bar{3}m$. The second discontinuity appearing in u and c/a at $V = 52.1 \text{ \AA}^3$ suggests a transition towards a third A7 variant where

the behavior of c/a and u is reversed; the 'cubic' value of $u = 0.25$ exactly, constant and independent of volume, and $c/a > \sqrt{6}$ and varying. So, allowing for the two structural degrees of freedom of $R\bar{3}m$, our calculations never converged towards a stable $cP1$ structure of Sb.

The non-smoothness of the $c/a(V)$ and $u(V)$ variations, occurring at essentially the same two volumes as marked by vertical lines in Fig. 8, was spotted in the context of comparisons of LDA vs: GGA calculations reported in Ref. 51. The details of the variations were not pursued throughout the "instability region", and Ref. 51 concluded at a phase transition to the $cP1$ structure at $V = 52 \text{ \AA}^3$ (incorrect), but found out that "the axial ratio converges to $c/a = \sqrt{6}$ before the parameter u converges to $u = 1/4$ " (correct). Another, more recent, calculation²⁸ concluded that the A7 \rightarrow Sb-II transition takes place at $P = 8.6 \text{ GPa}$, i.e. before the (hypothetical) A7 \rightarrow $cP1$ transformation might occur at the (calculated) pressure of $P = 10.7 \text{ GPa}$. Apparently, non-smooth variations of the A7 structure were not examined in detail in Ref. 28.

So as to estimate the uncertainties of our above procedures, we briefly compare the LDA calculations with the ones performed using the GGA. Within that approximation a similar behavior was obtained but the "coexistence region" of A7 variants is larger, i.e. $V = 52.2; 53.8 \text{ \AA}^3$. A sensible estimate is thus to situate the region of instabilities, which is to be compared to experiment, as the average of the two results: $V = 52.15; 53.35 \text{ \AA}^3$. Using then also for the $V \rightarrow P$ conversion the average of the LDA- and GGA-limits for $P(V)$, we obtain a lower "critical" pressure for the instability region as $P = 7.3 \text{ GPa}$. This is lower than the experimentally observed appearance of the Sb-II structure (8 to 8.5 GPa on upstroke). But, taking into account that the Sb-I to Sb-II transition exhibits a hysteresis of about 1 GPa at room temperature,^{8,26} the calculated critical pressure is only slightly less than the equilibrium transition pressure (roughly estimated as being the average pressure value for the upstroke and downstroke). So, there is not much room for actually finding an instability of the A7 phase preceding the Sb-I to Sb-II/IV transition.

In reports on early x-ray diffraction studies performed under non-hydrostatic conditions,⁵² the authors uphold to have observed the sluggish transformation to an intermediate primitive cubic structure of antimony in the pressure interval $P = 7.0; 8.5 - 9.0 \text{ GPa}$ or at least pronounced anomalies in the evolution of the A7 lattice parameters with pressure. The findings of Ref. 52, derived from low-resolution diffraction diagrams, have not been

confirmed in subsequent diffraction studies. Also, based on discontinuities in the pressure variation of the electrical resistivity of Sb seen at $P = 7.8 \text{ GPa}$ (upstroke) and 6.7 GPa (downstroke)²⁶ the existence of only one structural transition (A7 to Sb-II) is proposed in the interval considered here. Nevertheless, the parallel between our calculated results and the experimental observations of Ref. 52 is, perhaps, not accidental. It is conceivable that, in the presence of a substantial uniaxial stress component along the C_3 axis, a precursor transition can be induced. In this context it should be noted that, at fixed volume, the calculations yield optimized c/a ratios which are smaller than the experimental values [cf. Fig. 8(b)]. So, the condition of zero deviatoric stresses in the calculations corresponds to a strained configuration when compared to experimental data. With attention now being drawn to the importance of uniaxial stress, we arrive at what could be expected from intuition: the Peierls-like distortion of Sb-I, being a uniaxial effect, may depend sensitively on uniaxial stress along C_3 , with associated structural variations that are not observed under truly hydrostatic conditions.

To summarize, total energy calculations constrained to space group $R\bar{3}m$ point to the possible existence of an A7 to A7 transition near the borderline where antimony transforms to the higher-pressure Sb-II/IV phases. We do not rule out other modes of instability of the A7 structure that require a space group lower in symmetry (monoclinic) than $R\bar{3}m$. So, a more general conclusion would be that the 'normal' A7 structure of Sb may exhibit a structural instability before it transforms to the Sb-II/IV phases. Some tuning of the phase behavior through uniaxial stress may be possible. When comparing the calculations with experiment, an inherent uncertainty concerns the role played by a finite temperature. The present as well as other ab initio calculations of Sb were performed in the static lattice limit.

ACKNOWLEDGMENTS

We thank C. Ulrich for a critical reading of the manuscript. Part of the computer resources used in this work were provided by the Scientific Committee of IDRIS (Institut du Développement et des Ressources en Informatique Scientifique, Orsay, France).

Permanent address: Institut des Nanosciences de Paris, CNRS and Université Pierre and Marie Curie, 140 rue de Lourmel, F-75015 Paris, France

E-mail: k.syassen@fkf.mpg.de

¹ J. Donohue, The Structures of the Elements (J. Wiley & Sons, New York, 1974).

² D. Schiferl, D. T. Cromer, and J. C. Jamieson, Acta Cryst. B 37, 807 (1981).

³ K. Aoki, S. Fujwara, and M. Kusakabe, Solid State Commun. 45, 161 (1983).

⁴ H. Iwasaki and T. Kikigawa, Acta Cryst. B 53, 353 (1997).

⁵ M. I. McMahon, O. Dedyareva, and R. J. Nelmes, Phys.

- Rev. Lett. 85, 4896 (2000).
- ⁶ U. Schwarz, L. Akselrud, H. Rosner, A. Omeci, Y. Grin, and M. Han and, Phys. Rev. B 67, 214101 (2003).
 - ⁷ O. Dedyareva, M. I. Mamon, and R. J. Nelmes, High Press. Res. 24, 319 (2004).
 - ⁸ O. Dedyareva, M. I. Mamon, and R. J. Nelmes, Phys. Rev. B 70, 184119 (2004).
 - ⁹ K. J. Chang and M. L. Cohen, Phys. Rev. B 33, 7371 (1986).
 - ¹⁰ R. I. Sharp and E. Wamling, J. Phys. F 1, 570 (1971).
 - ¹¹ R. J. Needs, R. M. Martin, and O. H. Nielsen, Phys. Rev. B 33, 3778 (1986).
 - ¹² J. B. Renucci, W. Richter, M. Cardona, and E. Schonherr, phys. stat. sol. (b) 60, 299 (1973).
 - ¹³ J. S. Lannin, J. M. Calleja, and M. Cardona, Phys. Rev. B 12, 585 (1975).
 - ¹⁴ J. Hohne, U. W Enning, H. Schulz, and S. Hufner, Z. Physik B 27, 297 (1977).
 - ¹⁵ M. L. Bansal and A. P. Roy, Phys. Rev. B 33, 1526 (1986).
 - ¹⁶ T. K. Cheng, S. D. Brorson, A. S. Kazerooni, J. S. Moodera, G. D. Reselhaus, M. S. D. Reselhaus, and E. P. Ippen, Applied Physics Letters 57, 1004 (1990), see also G. A. Garrett, T. F. Albrecht, J. F. Whitaker, and R. Merlin, Phys. Rev. Lett. 77, 3661 (1996); T. E. Stevens, J. Kuhl, and R. Merlin, Phys. Rev. B 65, 144304 (2002); O. V. Misiho, M. Hase, and M. Katajima, J. Phys.: Condens. Matter. 16, 1879 (2004).
 - ¹⁷ W. Richter, T. Fjeldly, J. Renucci, and M. Cardona, in Proceedings of the International Conference on Lattice Dynamics, Paris, edited by M. Balkanski (Flammarion, Paris, 1978), p. 104.
 - ¹⁸ H. J. Beister, K. Strossner, and K. Syassen, Phys. Rev. B 41, 5535 (1990).
 - ¹⁹ M. Kasami, T. Mishina, and J. Nakahara, phys. stat. sol. (b) 241, 3113 (2004).
 - ²⁰ M. Kasami, T. Ogino, T. Mishina, S. Yamamoto, and J. Nakahara, J. Luminescence 119, 428 (2006).
 - ²¹ H. Schneider, W. Hafner, A. Wokaum, and H. Olijnyk, J. Chem. Phys. 96, 8046 (1992).
 - ²² G. J. Piermarini, S. Block, J. D. Barnett, and R. A. Forman, J. Appl. Phys. 46, 2774 (1975).
 - ²³ H. K. Mao, J. Xu, and P. M. Bell, J. Geophys. Res. 91, 4673 (1986).
 - ²⁴ Y. Grin, F. R. Wagner, M. Ambruster, M. Kohout, A. Leithe-Jasper, U. Schwarz, U. Wedig, and H. G. von Schnering, J. Solid State Chemistry 179, 1707 (2006).
 - ²⁵ W. Klement, Jr., A. Jayaraman, and G. C. Kennedy, Phys. Rev. 131, 632 (1963).
 - ²⁶ L. G. Khvostantsev and V. A. Sidorov, phys. stat. sol. (a) 82, 389 (1984).
 - ²⁷ J. Wittig, J. Phys. Chem. Solids 30, 1407 (1968), J. Wittig, in High Pressure Science and Technology, Proc. 9th AIRAPT Conference, MRS Symposia Proceedings, Vol. 22-II, North-Holland, New York, p.17.
 - ²⁸ U. Haussemann, K. Soderberg, and R. Norrestam, J. Am. Chem. Soc. 124, 15359 (2002).
 - ²⁹ A. Omeci and H. Rosner, Z. Krist. 219, 370 (2004).
 - ³⁰ J. F. Scott, Rev. Mod. Phys. 46, 83 (1974).
 - ³¹ L. M. Falicov and P. J. Lin, Phys. Rev. 141, 562 (1966).
 - ³² M. S. Dresselhaus, in The Physics of Semimetals and Narrow-Gap Semiconductors, edited by D. L. Carter and R. T. Bate (Pergamon, Oxford, 1971).
 - ³³ Y. Liu and R. E. Allen, Phys. Rev. B 52, 1566 (1995), see for references to related experimental and theoretical work.
 - ³⁴ M. Cardona and D. L. Greenaway, Phys. Rev. 133, A1685 (1964).
 - ³⁵ M. V. Klein, in Light Scattering in Solids III, edited by M. Cardona and G. Guntherodt (Springer, Berlin, 1982), vol. 8 of Topics in Applied Physics, p. 121.
 - ³⁶ C. Barrett, P. Cucka, and K. Haefner, Acta Crystallographica 16, 451 (1963).
 - ³⁷ S. Epstein and A. P. deBretteville, Phys. Rev. 138, A771 (1965).
 - ³⁸ R. F. S. Hearmon, Rev. Mod. Phys. 18, 409 (1946).
 - ³⁹ P. Hohenberg and W. Kohn, Phys. Rev. 136, B864 (1964).
 - ⁴⁰ W. Kohn and L. J. Sham, Phys. Rev. 140, A1133 (1965).
 - ⁴¹ P. E. Blochl, Phys. Rev. B 50, 17953 (1994).
 - ⁴² G. Kresse and D. Joubert, Phys. Rev. B 59, 1758 (1999).
 - ⁴³ G. Kresse and J. Hafner, Phys. Rev. B 47, R558 (1993); G. Kresse, Ph.D. Thesis, Technische Universität Wien (1993); G. Kresse and J. Furthmüller, Comput. Mater. Sci. 6, 15 (1996); G. Kresse and J. Furthmüller, Phys. Rev. B 54, 11169 (1996).
 - ⁴⁴ H. J. Monkhorst and J. D. Pack, Phys. Rev. B 13, 5188 (1976).
 - ⁴⁵ M. Methfessel and A. T. Paxton, Phys. Rev. B 40, 3616 (1989).
 - ⁴⁶ O. H. Nielsen and R. M. Martin, Phys. Rev. Lett. 50, 697 (1983), Phys. Rev. B 32, 3780 (1985).
 - ⁴⁷ J. P. Perdew and Y. Wang, Phys. Rev. B 45, 13244 (1992).
 - ⁴⁸ A. B. Shick, J. B. Ketterson, D. L. Novikov, and A. J. Freeman, Phys. Rev. B 60, 15484 (1999).
 - ⁴⁹ K. Kunc and P. G. Dacosta, Phys. Rev. B 32, 2010 (1985).
 - ⁵⁰ R. A. Cowley, Rep. Prog. Phys. 31, 123 (1968).
 - ⁵¹ K. Seifert, J. Hafner, J. Furthmüller, and G. Kresse, J. Phys.: Condens. Matter 7, 3683 (1995).
 - ⁵² T. N. Kolobyanina, S. S. Kabalkina, L. F. Vereshchagin, and L. V. Fedina, Zh. Eksp. Teor. Fiz. 55, 164 (1968), Engl. transl. in Soviet Phys. JETP 28, 88 (1969); see also L. F. Vereshchagin and S. S. Kabalkina, Zh. Eksp. Teor. Fiz. 47, 414 (1964), Engl. transl. in Soviet Phys. JETP 20, 274 (1965).